

A New Method for Selecting Exclusive Semileptonic Charmless B -Decays at e^+e^- Colliders at the $\Upsilon(4S)$

William S. Brower and Hans P. Paar¹

*Physics Department 0319, University of California at San Diego,
9500 Gilman Drive, La Jolla CA 92093-0319*

Abstract

We introduce a new method for selecting exclusive semileptonic charmless B -decays in the presence of a large background. The method can be applied to charged and neutral B -mesons decaying into any exclusive neutral or charged hadronic final state. The method is designed for high luminosity e^+e^- colliders operating at the $\Upsilon(4S)$. It employs an *improved* partial reconstruction technique for D^* -mesons and a novel 0- C event fit to *both* B -meson's decay products resulting in the kinematics of all particles (including neutrinos) in the event. The charged lepton energies are accessible from 1.0 GeV to the kinematic limit.

1 Introduction

Semileptonic B decays into charmless final states provide information about $|V_{ub}|$. Although the relation between $|V_{ub}|$ and the *exclusive* charmless semileptonic branching ratio is model dependent, this situation is improving as lattice calculation results become available [1]. In measuring the decay rates, it is desirable to sample as much of the kinematically allowed phase space as possible. This increases signal efficiency and allows to differentiate between theoretical models.

Branching fractions of exclusive semileptonic B decays into non-charm final states have been measured[2] to be approximately 2×10^{-4} . Because this small rate leads to a relatively large background from $b \rightarrow c$ decays and other sources, we have developed[3] a new method with excellent background rejection and acceptable signal efficiency. The method is based upon the kinematic

¹ Corresponding author, e-mail address: hpaar@ucsd.edu

reconstruction of the entire event with one B -meson decaying into the low rate channel of interest (the “signal”) and the other B -meson into a channel with a large branching fraction (the “tag”). The method can only be used at e^+e^- colliders that operate at the $\Upsilon(4S)$ center-of-mass energy because the kinematic reconstruction needs the magnitude of the B -meson’s momentum as an input. If the beams have a non-zero crossing angle or unequal energy the method applies after a transformation of all observed final state particles to the e^+e^- center of mass. The method can be used for charged and neutral B -mesons decaying into any exclusive neutral or charged hadronic final state. The method requires large luminosities such as will become available at B -Factories. The choice of a tag’s decay channel is dictated by the need to have a large branching fraction and a good detection efficiency. The decay $B \rightarrow D^*\ell\nu_\ell$ has the largest branching fraction but it has the disadvantage of introducing a second neutrino in addition to the neutrino on the signal side. As discussed in Sec. 2, events containing two exclusive semileptonic B decays can be reconstructed if all particles’ 3-momenta, except the two neutrinos, are measured.

To maintain efficiency, the D^* is reconstructed using an “*improved* partial reconstruction” technique that, like the “*standard* partial reconstruction” technique, only uses the pion kinematics from the decay $D^* \rightarrow D\pi$, see Sec. 3. The method is further improved by an novel 0- C event fitting procedure, introduced in Sec. 4.

2 Event Reconstruction

We consider the reconstruction of events of the type $B \rightarrow X\ell^+\nu_\ell$ (signal), $\overline{B} \rightarrow Y\ell^-\overline{\nu}_\ell$ (tag), where the B , \overline{B} , X , and Y may be charged or neutral. We assume that the momenta of the X , ℓ^+ , Y , and ℓ^- are measured. Particle masses are assigned according to the signal hypothesis. Incorrect assignments will generally cause the event to fail the procedure. Thus the energies of the four measured particles are known. The unknowns are the two angles associated with the direction of the back-to-back $B\overline{B}$ and the momenta of the two neutrinos, a total of 8. Energy-momentum conservation for each B decay gives 8 relations so the kinematics of all particles in the event (including the two neutrinos) can be calculated. Solutions come in pairs due to square-roots in the equations.

A geometric construction provides further understanding of the method and demonstrates its powerful rejection of background events owing to three requirements, see Fig. 1. The endpoint of the momentum vectors of the back-to-back B -mesons lie on the surface of a sphere of radius $325\text{ MeV}/c$ centered at their production point O (the “ $B\overline{B}$ sphere”). Starting with the B signal side,

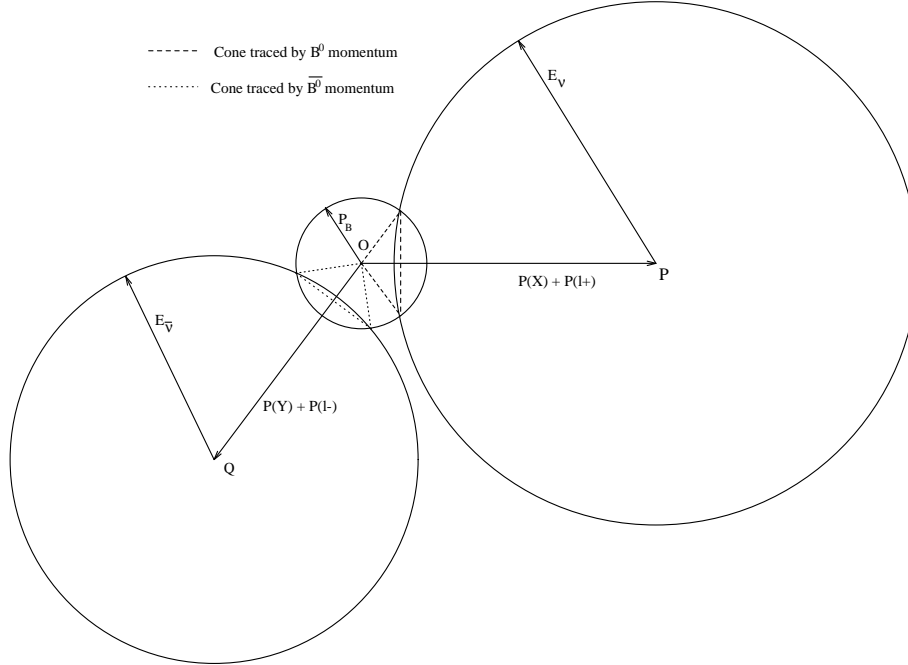


Fig. 1. Geometric construction that illustrates the event reconstruction of $B \rightarrow X\ell^+\nu_\ell$ and $\bar{B} \rightarrow Y\ell^-\bar{\nu}_\ell$.

the sum of the momenta of X and ℓ^+ is calculated and shown as the vector OP . Energy conservation applied to the B decay gives the neutrino energy $E_{\nu_\ell} = E_{beam} - \sqrt{\vec{p}_X^2 + m_X^2} - \sqrt{\vec{p}_{\ell^+}^2 + m_{\ell^+}^2}$. The neutrino momentum vector must lie on a sphere of radius E_ν centered on point P . *Constraint # 1*: require that this sphere and the $B\bar{B}$ -sphere intersect. The intersection is a circle perpendicular to OP on which the B momentum vector is constrained to lie. On the tag side, the sum of the momenta of Y and ℓ^- is calculated and shown as the vector OQ . The point Q is the center of a sphere with radius $E_{\bar{\nu}_\ell}$, calculated from energy conservation applied to the \bar{B} decay. *Constraint # 2*: require that this sphere and the $B\bar{B}$ -sphere intersect. The intersection is a circle perpendicular to OQ on which the endpoint of the \bar{B} momentum vector is constrained to lie. *Constraint # 3*: require that the B and \bar{B} momentum vectors, whose endpoints are constrained to lie on their respective circles, be back-to-back. To find the solution, reflect one of the circles through point O and find the intersection of the reflected circle and the other circle. If the circles intersect at all, there will be two intersections. Background events will generally not satisfy all three constraints.

To maintain acceptable efficiency for signal events, the D^* is not reconstructed from its $D\pi$ decay products: applicable branching fractions would cause an event loss of an order of magnitude. Instead the D^* kinematics are inferred from the kinematics of the π using the ‘‘partial reconstruction’’ technique. To have the best possible determination of the D^* kinematics (the other three particles are measured with negligible errors) for signal efficiency and back-

ground rejection we developed an *improved* partial reconstruction technique, to be discussed next.

3 Partial Reconstruction

Because the D^* - D mass difference is barely large enough to create a pion, the decay products in the $D^* \rightarrow D\pi$ decay have small momenta in the D^* center-of-mass system. This feature is exploited in the long known partial reconstruction technique[4] to get a *approximate* D^* momentum using only the pion's kinematics. Information on the D is not needed.

The energy in the laboratory of the D^* is given by

$$E_{D^*} = \frac{m_{D^*} E_\pi}{E_\pi^*} \frac{1}{1 + \beta_\pi^* \beta_{D^*} \cos \theta^*} \quad (1)$$

and the angle θ between the D^* and the π by

$$\tan \theta = \frac{E_\pi^* \sin \theta^*}{E_\pi} \frac{1 + \beta_\pi^* \beta_{D^*} \cos \theta^*}{\cos \theta^* + \beta_{D^*} / \beta_\pi^*} \quad (2)$$

Variables with a * are to be evaluated in the D^* center-of-mass system. In the *standard* partial reconstruction technique one sets $\beta_\pi^* = 0$. This gives

$$E_{D^*} = \frac{m_{D^*} E_\pi}{E_\pi^*} \quad (3)$$

and $\theta = 0$. A better approximation is obtained by studying the two-dimensional histogram of E_{D^*} and E_π , see Fig. 2, for the case $\bar{B}^0 \rightarrow D^{*+} \ell^- \bar{\nu}_\ell$, $D^{*+} \rightarrow D^0 \pi^+$. The ISGW[5] model was used to simulate the decays. The dots are the average D^* energy in each bin of p_π . The line represents Eq. (3). There is a significant difference between the dots and the line, especially at larger energies.

A lookup table can be constructed to obtain E_{D^*} from E_π (or p_π). We show in Fig. 3 the difference between the true E_{D^*} and E_{D^*} obtained with the *standard* partial reconstruction technique (solid histogram) and the *improved* partial reconstruction technique (dashed histogram) that uses such a lookup table. The improvement is clear. The improvement can be seen even more clearly in the difference between the true p_{D^*} and the partially reconstructed p_{D^*} , see Fig. 4 The rms deviation of this distribution decreased from 475 MeV/c to 330 MeV/c as a result of the improvement. The distribution of E_{D^*} energy in

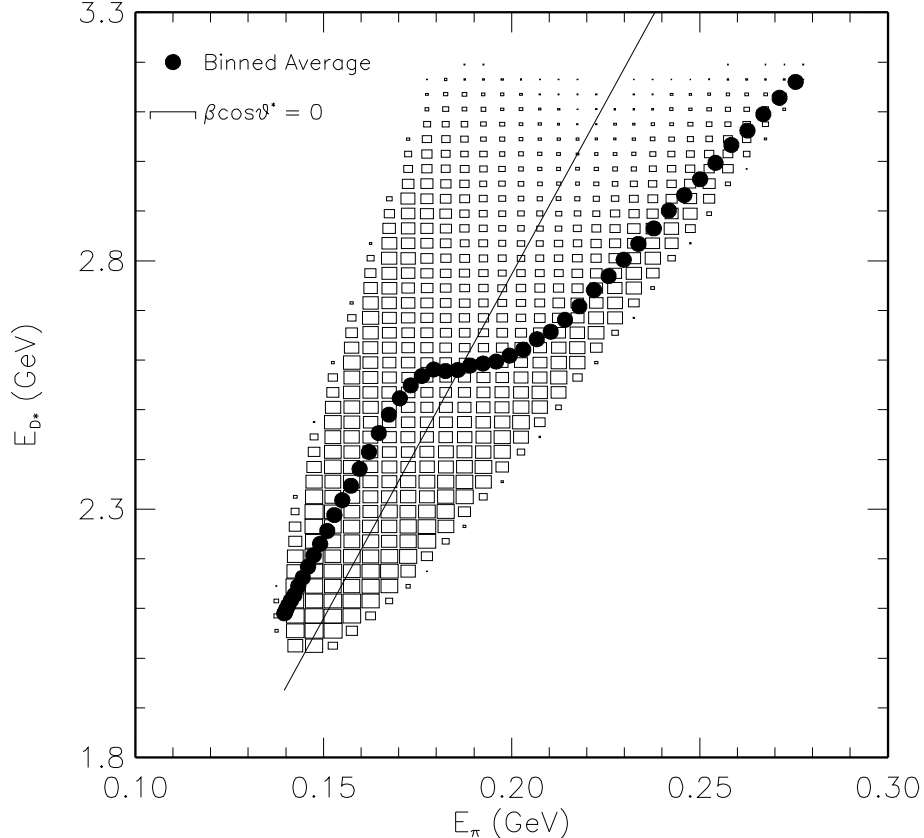


Fig. 2. Two-dimensional histogram of E_{D^*} and E_{π} in $\overline{B}^0 \rightarrow D^{*+} \ell^- \overline{\nu}_{\ell}$, $D^{*+} \rightarrow D^0 \pi^+$. The dots are the average D^* energy in each pion momentum bin. The line represents Eq. (3).

a given E_{π} bin is very skewed and for some applications the most probable instead of the mean may be more appropriate. A similar method may be used to improve the estimated direction of the D^* . We found that the benefits from improving the D^* direction are small.

In principle there is model dependence in the *improved* partial reconstruction technique. We have compared two models, ISGW[5] and ISGW2[6] that both describe the $B^0 \rightarrow D^{*+} \ell^- \overline{\nu}_{\ell}$ and found the difference between them to be negligible relative to their respective difference from the *standard* partial reconstruction.

4 Event Fit

Because the D^* momentum from *improved* partial reconstruction has an uncertainty of approximately 330 MeV/c, signal events may fail the event reconstruction. An example is shown in Fig. 5 where the solid sphere centered on point Q is the result of the *improved* partial reconstruction of the D^* while the

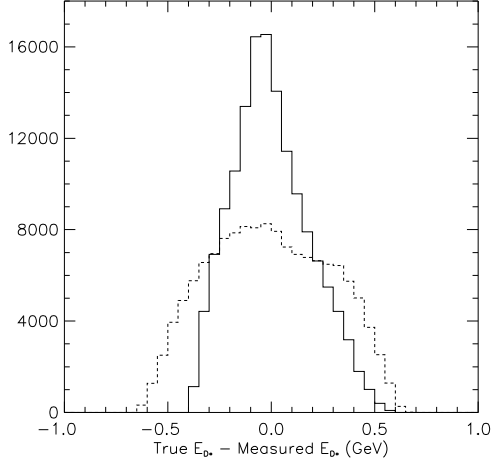


Fig. 3. Difference between true D^* energy and the D^* energy from partial reconstruction. The dashed histogram is for the *standard* and the solid histogram is for the *improved* partial reconstruction.

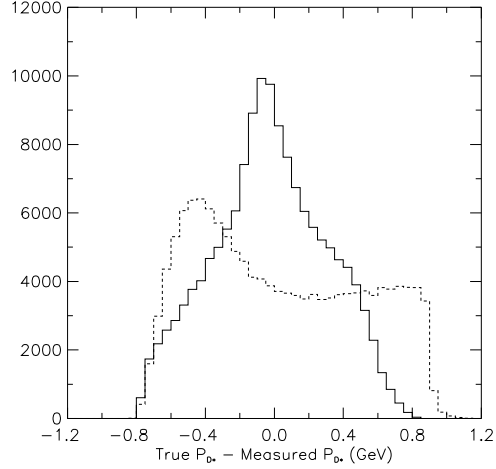


Fig. 4. Difference between true D^* momentum and the D^* momentum from partial reconstruction. The dashed histogram is for the *standard* and the solid histogram is for the *improved* partial reconstruction.

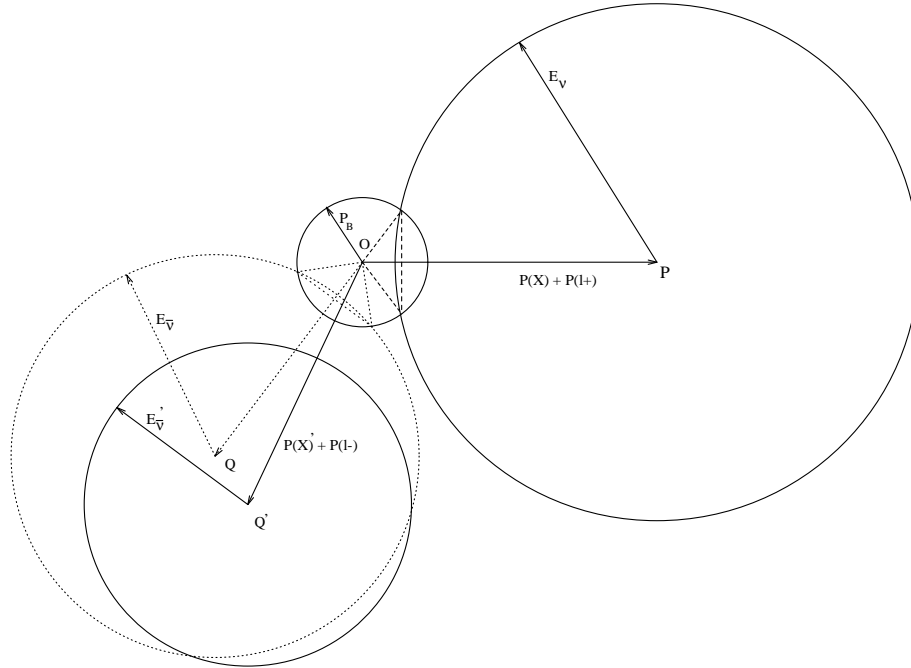


Fig. 5. The same event as in Fig. 1 showing that it now fails the event reconstruction because of the use of the partial reconstruction technique for the D^* . Point Q (Q') is the endpoint of the vector sum of the lepton and the true (partially reconstructed) D^* momentum.

true D^* leads to the dashed sphere centered on point Q. This is the same event as shown in Fig. 1. Now the event does not satisfy constraint #2 and would therefore be rejected as being background. It is possible to recover such signal events by varying the D^* momentum (causing Q' and $E'_{\bar{\nu}}$ to vary as well) such

that an intersection of the sphere centered on Q' and the $B\bar{B}$ sphere exists (constraint # 2) and that appropriate back-to-back B s exist (constraint # 3), see Sec. 2. This corresponds to performing a 0- C fit. Of all D^* momenta that satisfy the three constraints, we choose the one where the variation of the D^* momentum is minimal as measured by a χ^2 , defined as follows.

Using a model to simulate $B \rightarrow D^*\ell\nu$, $D^* \rightarrow D^0\pi$ we measured the covariance matrix V_{ij} defined as

$$V_{ij} = \frac{1}{N} \sum_{\text{events}} (p_{pr,i} - p_{tr,i})(p_{pr,j} - p_{tr,j}) \quad i, j = x, y, z \quad (4)$$

where p_{tr_i} (p_{pr_i}) is the i -th component ($i = x, y, z$) of the true (partially reconstructed) D^* momentum. Because there is significant dependence of the covariance matrix upon the pion momentum, it is measured in bins of pion momentum. A χ^2 is defined as

$$\chi^2 = \sum_i \sum_j (p_i - p_{pr,i})(V^{-1})_{ij}(p_j - p_{pr,j}) \quad i, j = x, y, z \quad (5)$$

where p_i is the i -th component of the D^* momentum. The D^* momentum with the lowest χ^2 and satisfying the three constraints is selected. For signal events, χ_{min}^2 is typically smaller than 1.0 while background events generally have very large χ_{min}^2 .

In Fig. 6 we show the difference between the true and the fitted D^* momentum (solid histogram). For comparison, we also show the difference of the true D^* momentum and the D^* momentum from respectively the *improved* (dashed histogram) and the *standard* (dotted histogram) partial reconstruction. Each histogram has the same number of events. The fit significantly improves the D^* kinematics, and that of its associated neutrino, thereby validating the fit procedure.

5 Results

The event reconstruction technique has been evaluated using simulated events. The simulation uses the ISGW model to describe exclusive semi-leptonic B decay and the detector simulation of the CLEOII detector[7]. The simulation is known to describe the detector response well. The simulation generates raw data in the same format as real data. The simulated raw data are processed through the same analysis procedures as the real data. For definiteness we limit the discussion that follows to the reactions $B^0 \rightarrow \pi^- \ell^+ \nu_\ell$ (signal), $\bar{B}^0 \rightarrow D^{*+} \ell^- \bar{\nu}_\ell$ (tag) with $D^{*+} \rightarrow D^0 \pi^+$.

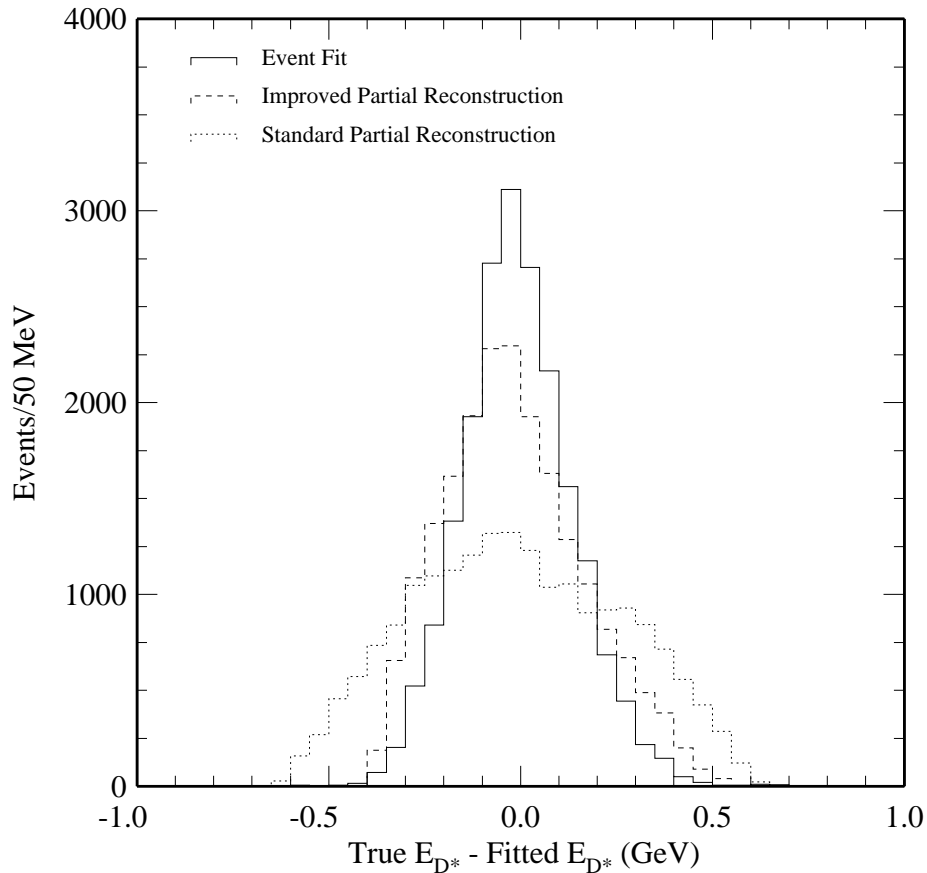


Fig. 6. Difference between the true and the fitted D^* energy (solid histogram). Also shown are the difference between the true D^* momentum and the D^* momentum from respectively the *improved* (dashed histogram) and the *standard* (dotted histogram) partial reconstruction.

A detailed discussion of the analysis is outside the scope of this paper. Briefly, events with at least 4 charged tracks are selected, two of which must be leptons with momenta greater than $1.0 \text{ GeV}/c$. The leptons can have opposite or equal charges because of $B^0-\bar{B}^0$ mixing. At least one of the other two tracks must have a momentum between 40 and $200 \text{ MeV}/c$, the kinematically allowed range for the pion from D^{*+} decay. The most important background process is the one in which the signal B also decays into a charmed final state. To suppress this background at least partly, we calculate the effective mass and the total momentum of unused tracks and energy deposits in the electromagnetic calorimeter. For signal events all unused tracks and energy deposits are the result of D^0 decay so if their effective mass is greater than the D^0 mass the event is rejected. Likewise, if the angle in the laboratory between their total momentum and the pion momentum is greater than 37 deg , the event is rejected.

With this event selection, we loop over all combinations of four tracks in an event and over all events and apply the $0-C$ event fit and the *improved*

partial reconstruction. The resulting χ_{\min}^2 distribution is shown for signal and background events in Fig. 7. The latter are $B\bar{B}$ events that decay according to known decay modes, not including semi-leptonic charmless decays. When

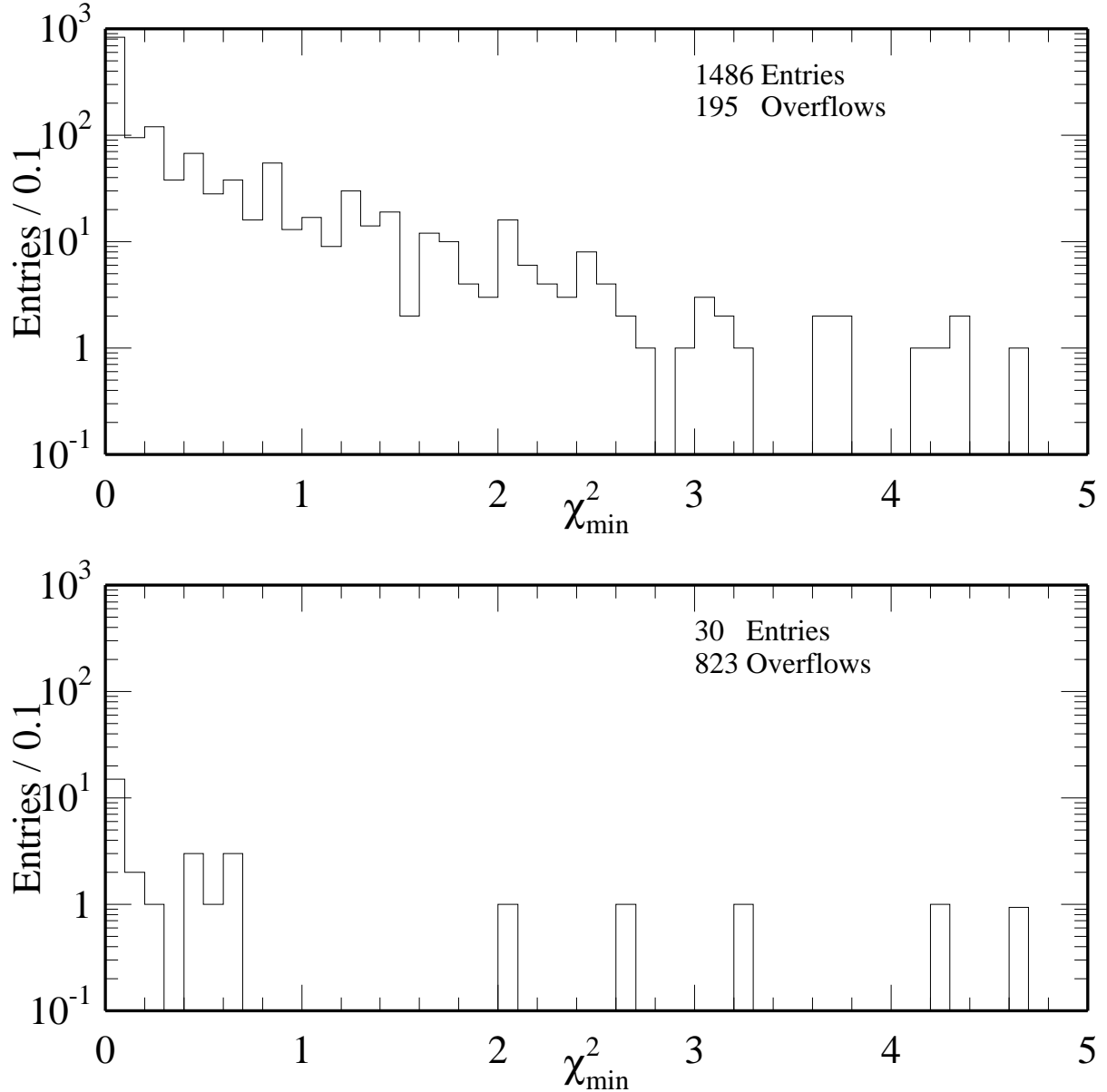


Fig. 7. χ_{\min}^2 distributions for simulated signal (top) and background (bottom) events. Note the logarithmic scale and the number of overflow events in each case.

we require $\chi_{\min}^2 \leq 1.0$, only 19 out of 853 background events pass, a rejection factor of 45.

The signal efficiency ϵ , defined to include the branching fraction $B(D^{*+} \rightarrow D^0\pi^+) = 0.68$, is measured to be 3.66%. The number of signal events is

expected to be

$$N = 21 \left(\frac{L}{1 \text{ fb}^{-1}} \right) \left(\frac{B(B^0 \rightarrow \pi^- \ell^+ \nu_\ell)}{1.0 \times 10^{-4}} \right) \epsilon \quad (6)$$

where L is the integrated luminosity. The numerical factor includes the $\overline{B}^0 \rightarrow D^{*+} \ell^- \overline{\nu}_\ell$ branching fraction and the $B\overline{B}$ production cross section. B -factories aim for integrated luminosities of at least $30 \text{ fb}^{-1}/\text{year}$. A branching fraction $B(B^0 \rightarrow \pi^- \ell^+ \nu_\ell) = 2 \times 10^{-4}$ [2] would result in about 50 events per signal channel with about 20 events background. When several signal channels are combined these numbers are expected to give measurements of $|V_{ub}|$ whose precision is dominated by theoretical uncertainties. A vertex detector would improve the tracking of low momentum particles (important for partial reconstruction) and allow the rejection of some of the remaining charm background. As indicated earlier, the method can be applied to charged and neutral B s decaying into any exclusive neutral or charged hadronic final states, allowing many measurements of $|V_{ub}|$.

Acknowledgements

The authors thank their CLEO colleagues for the use of the CLEO analysis and event simulation code and the CLEO Monte Carlo dataset. We have greatly benefitted from many fruitful discussions with colleagues interested in semileptonic B -meson decays.

References

- [1] C. R. Allton *et al*, Phys. Lett. B **345**, 513 (1995); L. Lellouch, hep-ph/9609501 and references therein.
- [2] J.P. Alexander *et al*, (CLEO Collaboration), Phys. Rev. Lett. **77**, 5000 (1996).
- [3] W.S. Brower, PhD Thesis (1996), UC San Diego, La Jolla CA 92093-0319, unpublished.
- [4] Reference to first delta-m paper.
- [5] N. Isgur, D. Scora, B. Grinstein, and M.B. Wise (ISGW), Phys. Rev. D **39**, 799 (1989).
- [6] D. Scora and N. Isgur (ISGW2), CEBAF Theory Group Preprint CEBAF-TH-94-14 (1994), hep-ph/9503486.
- [7] Y. Kubota *et al* (CLEO Collaboration), Nucl. Instr. Meth. A **320**, 66 (1992).